Regenerative Therapy 24 (2023) 536–546

Contents lists available at ScienceDirect

Regenerative Therapy

journal homepage: http://www.elsevier.com/locate/reth

Original Article

Modeling of intramembranous ossification using human pluripotent stem cell-derived paraxial mesoderm derivatives

Yuki Ikeda [a, b], Shoichiro Tani [c], Takeshi Moriishi [d], Aiko Kuroda [d], Yuki Matsuo [d], Naoya Saeki [a], Chizuko Inui-Yamamoto [a], Makoto Abe [a], Takashi Maeda [a], David W. Rowe [e], Ung-il Chung [c], Hironori Hojo [c], Yuki Matsushita [d], Takashi Sawase [b], Shinsuke Ohba [a, *]

[a] Department of Tissue and Developmental Biology, Graduate School of Dentistry, Osaka University, Osaka 565-0871, Japan
[b] Department of Applied Prosthodontics, Graduate School of Biomedical Sciences, Nagasaki University, Nagasaki 852-8588, Japan
[c] Laboratory of Clinical Biotechnology, Center for Disease Biology and Integrative Medicine, Graduate School of Medicine, The University of Tokyo 113-8655, Japan
[d] Department of Cell Biology, Graduate School of Biomedical Sciences, Nagasaki University, Nagasaki 852-8588, Japan
[e] Department of Reconstructive Sciences, University of Connecticut Health Center, CT 06030, USA

ARTICLE INFO

Article history:
Received 27 August 2023
Received in revised form
25 September 2023
Accepted 28 September 2023

Keywords:
Human pluripotent stem cells
Paraxial mesoderm
Intramembranous ossification
Endochondral ossification
Osteoblast
Osteocyte

ABSTRACT

Vertebrates form their skeletal tissues from three distinct origins (the neural crest, paraxial mesoderm, and lateral plate mesoderm) through two distinct modes of ossification (intramembranous and endochondral ossification). Since the paraxial mesoderm generates both intramembranous and endochondral bones, it is thought to give rise to both osteoprogenitors and osteo-chondroprogenitors. However, it remains unclear what directs the paraxial mesoderm-derived cells toward these different fates in distinct skeletal elements during human skeletal development. To answer this question, we need experimental systems that recapitulate paraxial mesoderm-mediated intramembranous and endochondral ossification processes. In this study, we aimed to develop a human pluripotent stem cell (hPSC)-based system that models the human intramembranous ossification process. We found that spheroid culture of the hPSC-derived paraxial mesoderm derivatives generates osteoprogenitors or osteo-chondroprogenitors depending on stimuli. The former induced intramembranous ossification, and the latter endochondral ossification, in mouse renal capsules. Transcriptional profiling supported the notion that bone signatures were enriched in the intramembranous bone-like tissues. Thus, we developed a system that recapitulates intramembranous ossification, and that enables the induction of two distinct modes of ossification by controlling the cell fate of the hPSC-derived paraxial mesoderm derivatives.

1. Introduction

Vertebrates form their skeletal tissues from three distinct origins: the neural crest, paraxial mesoderm, and lateral plate mesoderm [1]. Neural crest- and paraxial mesoderm-derived skeletal progenitors undergo both intramembranous and endochondral ossification, while lateral plate mesoderm-derived ones undergo only endochondral ossification [2]. Endochondral ossification begins with mesenchymal condensation; skeletal progenitors in the condensed mesenchyme initially differentiate into chondrocytes, which generate the cartilage template. Cells around the template then differentiate into bone-forming osteoblasts, which gradually replace cartilage with bone in conjunction with blood vessel invasion. In intramembranous ossification, skeletal progenitors in condensed mesenchyme directly differentiate into osteoblasts, which form bones without the cartilage template [2]. Intramembranous ossification is observed in the facial bones, cranial vault, and a portion of the clavicle, whereas endochondral ossification is found in the limb skeleton, most of the axial skeleton, and the skull base [2].

* Corresponding author. Department of Tissue and Developmental Biology, Graduate School of Dentistry, Osaka University, 1-8 Yamadaoka, Suita, Osaka 565-0871, Japan.
E-mail address: ohba.shinsuke.dent@osaka-u.ac.jp (S. Ohba).
Peer review under responsibility of the Japanese Society for Regenerative Medicine.

https://doi.org/10.1016/j.reth.2023.09.017

Paraxial mesoderm, one of the skeletal origins, gives rise to the sclerotome and dermomyotome via the somites [3]. The sclerotome contains skeletal progenitors, which contribute to a variety of skeletal elements in the craniofacial (the parietal and occipital bones) and axial regions, whereas the dermomyotome gives rise to the dermis and muscles [3]. Given that the paraxial mesoderm generates both intramembranous and endochondral bones, the paraxial mesoderm-derived skeletal progenitors are thought to have the ability to become both osteoprogenitors and osteo-chondroprogenitors. However, it remains unclear what determines their behaviors in distinct skeletal elements during human skeletal development. To answer the question, we need experimental systems that recapitulate paraxial mesoderm-mediated intramembranous and endochondral ossification processes.

There have been a number of studies using the pluripotent stem cell (hPSC)-derived paraxial mesoderm and its derivatives, i.e., the sclerotome, to model skeletal development (reviewed in Refs. [4,5]); most of these studies have focused on recapitulating endochondral ossification [6–10]. At least two studies showed direct differentiation of hPSC-derived paraxial mesoderm and sclerotome into osteoblasts [11,12]; however, the induced cells did not undergo intramembranous ossification in a three-dimensional (3D) manner. In this context, we recently developed a hPSC-based organ modeling system that recapitulated the endochondral ossification process along the paraxial mesoderm–sclerotome axis [13]. In brief, hPSCs were differentiated *in vitro* into sclerotome via the paraxial mesoderm and somites in a stepwise manner; endochondral bones were generated by implanting hPSC-derived sclerotome into mouse renal capsules. This result indicates that the hPSC-derived sclerotome population is programmed to become osteo-chondroprogenitors directing endochondral ossification as a default setting, in the same way that the sclerotome does in *in vivo* skeletal development. Here we hypothesized that if we could direct the population toward the osteoprogenitor fate, we would be able to recapitulate the 3D intramembranous ossification process using the mouse renal capsule system.

In this study, we aimed to develop a hPSC-based system that models the human intramembranous ossification process. By optimizing the culture conditions, we found that the 3D spheroid culture of the hPSC-derived sclerotome population generated osteoprogenitors and osteo-chondroprogenitors depending on stimuli. The former induced intramembranous ossification, and the latter endochondral ossification, in mouse renal capsules. Transcriptional profiling supported the notion that bone signatures were enriched in the intramembranous bone-like structures. Thus, we developed a system that recapitulates intramembranous ossification, and that enables the induction of two distinct modes of ossification by controlling the cell fate of the hPSC-derived sclerotome.

2. Methods

2.1. Sclerotome induction

We utilized the following human induced pluripotent stem cells (hiPSCs) and human embryonic stem cells (hESCs): hiPSC-1 [13], Col2.3GFP-H9-hESCs [13,14], and WIZ04e-H9CAGmChry-hESCs (obtained from WiCell Research Institute, Madison, WI) [15]. These hPSCs were adapted and maintained by a xeno-free culture system using Essential 8 medium (#A1517001; Thermo Fisher Scientific Inc., Waltham, MA) on recombinant human vitronectin (VTN: #A14700; Thermo Fisher Scientific Inc.)-coated plates. hPSCs were maintained in 6-well plates up to 60% confluency. Sclerotome induction was achieved by 5-day treatment with small-molecules as previously described [13]. Briefly, cells were cultured in BIM medium, which consists of DMEM/F12 (#D8062; Sigma-Aldrich/Merck, Burlington, MA) supplemented with 1% MEM Non-Essential Amino Acids (#11140050; Thermo Fisher Scientific), 55 μM 2-mercaptoethanol (#21985023; Thermo Fisher Scientific), B-27 Supplement Xeno-free (#A14867-01; Thermo Fisher Scientific), and 1% ITS Liquid Media Supplement (#13146; Sigma-Aldrich/Merck), and subjected to the following induction protocol. The first 24-h treatment with CHIR99021 (5 μM: #034-23103; FUJIFILM Wako Pure Chemical Corporation, Osaka, Japan) induced the cells into the primitive streak. The next 24-h treatment with CHIR99021 (5 μM), A-83-01 (1 μM: #2939; Tocris Bioscience, Bristol, UK), and LDN193189 (0.25 μM: #SML0559; Sigma-Aldrich/Merck) induced the cells into paraxial mesoderm. To induce somites, the cells were then treated with C59 (1 μM: #C7641-2; Cellagen Technology, San Diego, CA), A-83-01 (1 μM), and LDN193189 (0.25 μM) for 24 h. Lastly, the cells were differentiated into sclerotome by 48-h treatment with C59 (1 μM), SAG (1 μM: #566660; Calbiochem, Darmstadt, Germany), and LDN (0.25 μM).

2.2. Skeletal progenitor induction

Sclerotome cells were dissociated from the plates using Accutase (#AT104; Innovative Cell Technologies, San Diego, CA). 1.0×10^4 cells were plated in each well of v-bottom shaped low-adhesive spheroid plates (MS-9096V; Sumitomo Bakelite, Tokyo) or v-bottom shaped plates coated with 0.5% Lipidure (CM5206; NOF Corp., Tokyo) in ethanol, and cultured as spheroids for an additional 14 days (from Day 5 to Day 19) in the BIM medium with or without SAG and TH (a helioxanthin derivative, 4-(4-Methoxyphenyl)thieno [2,3-*b*:5,4-*c'*]dipyridine-2-carboxamide: #M3085; Tokyo Chemical Industry, Tokyo). The medium was changed once at Day 12.

2.3. Reverse-transcription quantitative polymerase chain reaction (RT-qPCR)

Total RNA was extracted using ISOGEN (#319-90211; Nippon Gene, Tokyo) and an RNeasy Mini Kit (74104; Qiagen, Hilden, Germany) according to the manufacturer's instructions. After measurement of the RNA concentration, reverse transcription was performed using ReverTra Ace qPCR RT Master Mix with gDNA Remover (#FSQ-301; TOYOBO, Osaka, Japan). The PCR reaction mixture was composed of THUNDERBIRD SYBR qPCR Mix (#QPS-201; TOYOBO) or Taq Pro Universal SYBR qPCR Master Mix (#Q712-02; Nanjing Vazyme Biotech, Nanjing, China), 10 μM of specific primers, and cDNA. qPCR was performed with a LightCycler 480 system or LightCycler 96 Instrument (Roche, Basel, Switzerland) under the following conditions: 40 cycles of 95 °C for 10 s and 60 °C for 30 s. Relative expression levels were calculated by ddCt methods [16] using *RPS13* as an internal control and Day 0 expression as a calibrator. The primer sequences are listed in Supplementary Table 1.

2.4. Renal capsule implantation

After the induction culture, the spheroids were resuspended in fresh BIM medium (usually 8–16 spheroids per tube). The spheroids suspension was diluted with an equal amount of Matrigel (#354234; Corning, Somerville, MA). For renal capsule implantation of the spheroids, 8- to 12-week-old immunodeficient male mice (CB-17/Icr-scid/scidJcl; CLEA Japan, Tokyo) were anesthetized with intraperitoneal injection of a mixture of medetomidine (0.3 mg/kg body weight), midazolam (4 mg/kg body weight), and butorphanol (5 mg/kg body weight) [17]. We made an

approximately 10 mm skin incision, cut the peritoneum, and gently squeezed out the kidney from the incision site. An aliquot of the spheroid suspension (100–200 μL per kidney) was injected underneath the renal capsule of the mice using 26G needles and syringes. The peritoneum and skin were separately sutured with 6-0 nylon. At 8 and 12 weeks after implantation, the kidneys were harvested and fixed with 4% paraformaldehyde (PFA: 02890-45; Nacalai Tesque, Kyoto, Japan)/phosphate-buffered saline (PBS without calcium and magnesium) overnight at 4 °C for the subsequent analyses shown below. All experiments were performed in accordance with the protocols approved by the Animal Care and Use Committee of Osaka University (R-04-009-0) and Nagasaki University (#1909101567). Mice were kept in individual cages under controlled temperature and humidity with a 12-h circadian rhythm and were given ad libitum access to food and water. All efforts were made to minimize the suffering of the mice.

2.5. Three-dimensional micro-computed tomography (CT) analysis (3D-μCT)

The reconstructed images of 3D-μCT were obtained using a Skyscan 1272 μCT scanner (Bruker, Billerica, MA) at a resolution of 3.75 μm/pixel.

2.6. Histological analysis

Decalcification was performed with 0.5 M ethylenediaminetetraacetic acid (EDTA)/PBS (PH 7.4) at 4 °C for two days. Decalcified samples were kept in 30% sucrose/PBS for 2 h at 4 °C. The samples were then incubated in O.C.T. Compound (Sakura Finetek Japan, Tokyo) at 4 °C for 1 h and embedded in O.C.T. Compound. Frozen sections were cut at 5 μm with a Leica CM3050 S Cryostat (Leica Biosystems, Wetzlar, Germany). Prior to staining, the sections were washed with PBS at room temperature (RT) for 5 min. For hematoxylin and eosin (H-E) staining, the sections were immersed in Mayer's hemalum solution (#109249; Sigma-Aldrich/Merck) for 1 min, washed with tap water for 10 min, and subsequently immersed in 0.2% eosin/ethanol for 1 min. The stained sections were immersed in ethanol and xylene for dehydration, and then mounted with Malinol (#2009-2; Muto Pure Chemicals, Tokyo). For Safranin-O staining, the sections were immersed in 0.5% hematoxylin for 1 min, washed with tap water for 3 min, immersed in 0.05% Fast Green (#F0718; Tokyo Chemical Industry) for 5 min, rinsed quickly with 1% acetic acid, and immersed in 0.1% safranin O (#11500; Chroma-Gesellschaft Schmid GmbH & Co. KG, Stuttgart, Germany) for 5 min. The stained sections were dehydrated and mounted.

2.7. Immunohistochemistry

For immunofluorescence, frozen sections were briefly washed with 0.1% TritonX-100/PBS (PBST) and blocked with 3% bovine serum albumin (#A7906; Sigma-Aldrich/Merck) and 0.1% heat inactivated sheep serum (S-2263; Sigma-Aldrich/Merck) in PBST at RT for 1 h. The blocked sections were incubated with primary antibodies diluted in the blocking solution at 4 °C overnight. After being washed with PBST, the sections were incubated with Alexa Fluor® 488 goat anti-rabbit IgG (H + L) (#A-11034; Thermo Fisher Scientific) at RT for 1 h. After an additional washing with PBST, the sections were mounted with VECTASHIELD Antifade Mounting Medium with DAPI (#H-1200; Vector Laboratories, Newark, CA). Coverslips were fixed with nail polish.

For chromogenic immunohistochemistry using 3,3′ diaminobenzidine (DAB), endogenous peroxidase activity was quenched by immersing sections in 0.3% hydrogen peroxide/methanol for 30 min at RT prior to the blocking step. After incubation with primary antibodies and washing with PBST as described above, the sections were incubated with ready-to-use HRP-conjugated secondary antibodies (SignalStain Boost IHC Detection Reagents: #8125 and #8114 for mouse and rabbit primary antibodies, respectively; Cell Signaling Technology, Danvers, MA) at RT for 1 h. DAB staining was performed using a DAB substrate kit (#SK-4100; Vector Laboratories) according to the manufacturer's protocols. Counterstaining was performed by dipping sections in Mayer's hemalum solution (#109249; Sigma-Aldrich/Merck) for 30 s. After washing with tap water, the sections were mounted with 50% glycerol. Images were obtained using a BZ-X800 microscope (Keyence, Osaka, Japan). Primary antibodies used in this study are listed in Supplementary Table 2.

2.8. In situ *hybridization*

Non-radioactive *in situ* hybridization was performed as previously described [18,19]. We used DIG RNA labeling mix (#1277073; Roche) to synthesize digoxigenin (DIG)-labeled antisense probes corresponding to mouse *Col1a1* (NM_007742.4; nt.3001-3461) [20], mouse *Col2a1* (NM_031163.4; nt.4334-4642) [18], and human *SOST* (NM_025237.3; nt.1258-1792) sequences. In brief, fixed sections were treated with 1 μg/mL proteinase K (#9033; Takara Bio Inc., Shiga, Japan) for 6 min at RT, refixed with 4% PFA/PBS, washed with PBS, acetylated for 15 min at RT, washed again with PBS, and prehybridized for 30 min at 60 °C in hybridization buffer containing 50% formamide, 5 X SSC (pH 4.5), 50 μg/mL yeast tRNA (#R8759; Sigma-Aldrich/Merck), 1% sodium dodecyl sulfate (SDS), and 50 μg/mL heparin (#17513-41; Nacalai Tesque). The sections were then hybridized with the DIG-labeled probes in hybridization buffer overnight at 60 °C or 70 °C. After hybridization, the sections were washed with 4 x SSC once and subsequently with 0.2 x SSC twice. Hybridization was visualized using anti-DIG-AP antibodies (1:5000; #11093274910; Roche) combined with BM-Purple (#11442074001; Roche) according to the manufacturer's instructions. Counterstaining was performed with Fast Red.

2.9. Bulk RNA-sequence (RNA-seq) analysis

For Day 0 (pluripotent state) and Day 5 (sclerotome) samples, total RNA was obtained from cultured cells as described earlier. *In vivo* induced tissues were harvested from kidney capsules and homogenized in ISOGEN; the homogenized samples were then subjected to total RNA isolation. Total RNA samples were submitted to Takara Bio Inc. for library construction and sequencing. The RNA-seq library was constructed by using a SMART-Seq v4 Ultra Low Input RNA kit (Takara Bio Inc.). Paired-end sequencing (2 × 150 bp) was performed by using a Novaseq 6000 system (Illumina, San Diego, CA) with a sequencing depth of 40 million reads per sample. Biological replicates were analyzed for each group (N = 3); for *in vivo* induced tissues, three independent tissue clumps were analyzed as biological replicates. The quality of the sequencing reads was checked by FastQC, and the reads were processed by Trimmomatic [21]. The processed reads were aligned to the hg38 reference genome using the STAR aligner [22]. Quantification of gene expression and differentially expressed gene analysis were performed by featureCounts [23] and DESeq2 [24], respectively. iDEP.96 [25] was used for the principal component analysis, volcano plot, and k-means clustering. Gene ontology analysis was performed using the ShinyGO 0.77 analysis tool [26]. The RNA-seq data obtained in this study are available at DNA Data Bank of Japan (DDBJ) under the BioProject accession number PRJDB16436 (DRA016948, DRA016949, DRA016950, DRA016951, DRA016952, DRA016953, DRA016954, DRA016955, and DRA016956).

2.10. Statistical analysis

In Fig. 1, the data are expressed as mean ± standard deviation (SD). Statistical data analyses were performed using BellCurve for Excel. Statistical significance was determined by Dunnett's test or a one-way ANOVA followed by Tukey's multiple comparisons test. The tests used in each experiment are described in the figure legends. P-values <0.05 were considered to be statistically significant.

3. Results

3.1. Establishment of the in vitro protocol for generating skeletal progenitors from hPSC-derived sclerotome

We recently reported a stepwise protocol for inducing a sclerotome population from hPSCs via the paraxial mesoderm and somites [13]. We cultured a hiPSC line (hiPSC-1; see the Methods

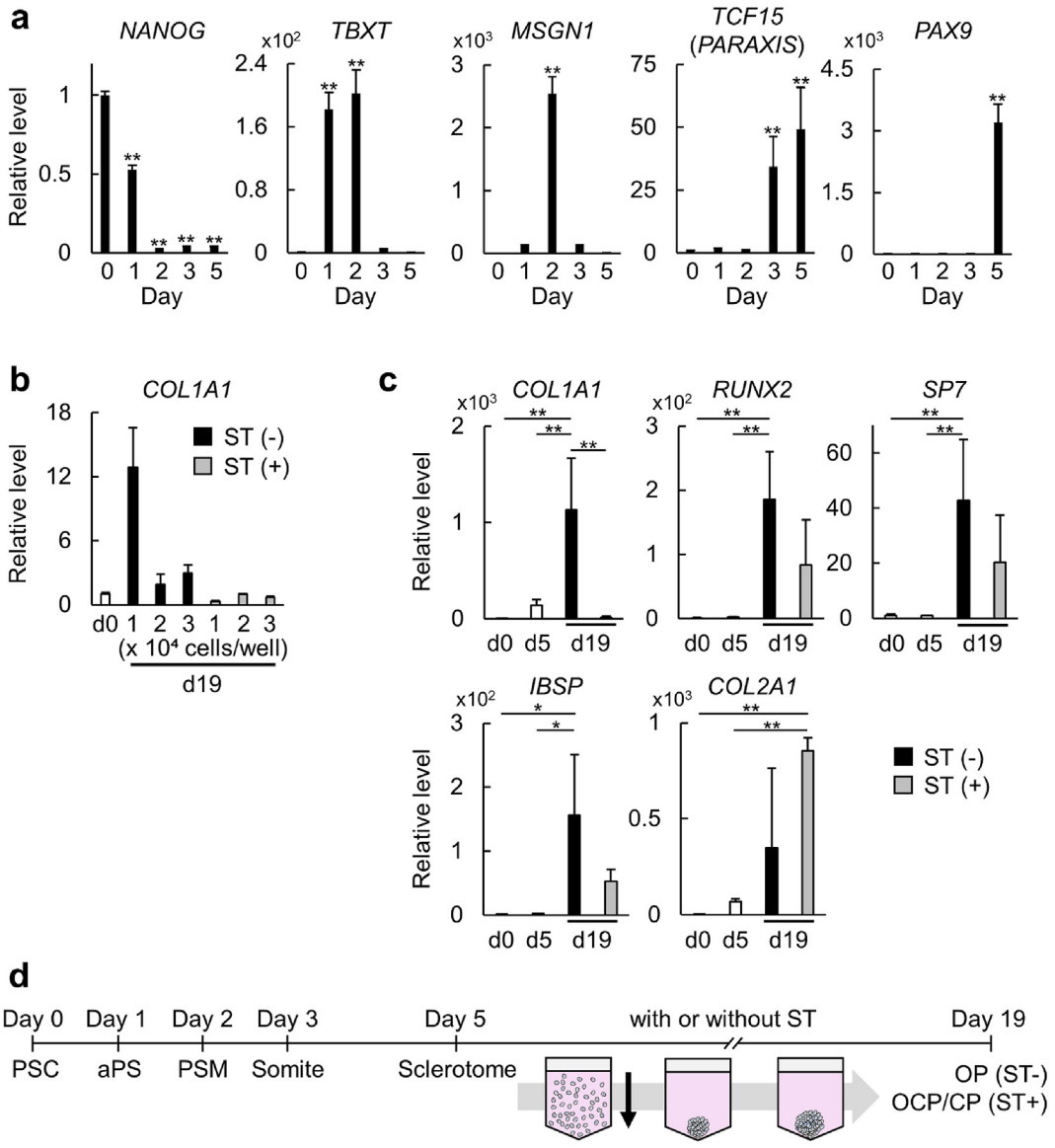

Fig. 1. *In vitro* induction of the hPSC-derived sclerotome population into skeletal progenitors. (a) Confirmation of the stage-specific marker gene expression during sclerotome induction. hiPSCs were cultured according to a sclerotome induction protocol (see the main text). The mRNA expression was determined by RT-qPCR on the indicated days of the culture. The data are expressed as the mean ± SD from triplicate samples. **p < 0.01 vs. Day 0 (Dunnet's test). (b) The expression of osteoblast-related genes in the 3D induction (spheroid) culture of the hiPSC-derived sclerotome population. Following the 5-day sclerotome induction, the indicated numbers of hiPSC-derived cells were plated on each well of spheroid plates and cultured with or without SAG + TH (ST) for another 14 days (until Day 19). The mRNA expression of *COL1A1* was determined by RT-qPCR on Days 0 and 19. The data are expressed as the mean ± SD from triplicate samples. No statistical significance was detected by Tukey's multiple comparisons test. (c) The expression of skeletal genes in the spheroid culture of the hiPSC-derived sclerotome population. Following the 5-day sclerotome induction, 10,000 cells/well were subjected to the 14-day spheroid culture (until Day 19). The mRNA expression was determined by RT-qPCR on Days 0, 5, and 19. The data are expressed as the mean ± SD from triplicate samples. *p < 0.05 and **p < 0.01 (Tukey's multiple comparisons test). (d) A schematic showing the optimized protocol for generating osteoprogenitors (OP) under the ST (−) condition and osteo-chondroprogenitors/chondroprogenitors (OCP/CP) under the ST (+) condition from the hiPSC-derived sclerotome population *in vitro*.

section) according to the induction protocol, in order to obtain the hPSC-derived sclerotome. During the induction culture, the expression patterns of the genes *NANOG*, *TBXT*, *MSGN1*, *TCF15* (*PARAXIS*), and *PAX9* were determined as markers for the pluripotent state, primitive streak, paraxial presomitic mesoderm, somite, and sclerotome, respectively (Fig. 1a); they showed stage-specific expression pattens, indicating successful sclerotome induction in this study (Fig. 1a).

Following sclerotome induction, we tried to induce skeletal progenitors *in vitro*. We previously found that the combination of the smoothened agonist (SAG), which activates Hedgehog signaling, and the osteogenic small compound TH differentiated hiPSC-derived mesoderm and mouse mesenchymal cells into osteoblastic cells [27–30]; the combination is called ST hereafter. Given that both modes of ossification begin with mesenchymal condensation, we then hypothesized that 3D spheroid cultures, which potentially mimic mesenchymal condensation, would augment skeletal progenitor induction from the hiPSC-derived sclerotome in the presence of ST. Utilizing low-adhesive 96-well plates to facilitate spheroid formation, we screened an appropriate seeding cell number ($1.0–3.0 \times 10^4$ cells) and stimuli (with or without ST) in the 14-day spheroid culture of hiPSC-derived sclerotome. The osteoblast-related gene *COL1A1* was upregulated at the highest level in the 1.0×10^4 group cultured without ST (Fig. 1b), although the difference was not statistically significant. Therefore, we adopted 1.0×10^4 cells as the seeding cell number and further examined the expression of a series of skeletal genes in the culture with or without ST. The ST (−) group, but not the ST (+) group, showed significant upregulation of osteoblast-related genes (*COL1A1*, *RUNX2*, *SP7*, and *IBSP*) compared to Day 0 (a pluripotent state) and Day 5 (sclerotome) (Fig. 1c); importantly, the ST (−) group showed significantly higher expression of *COL1A1* and trends toward upregulation of *RUNX2*, *SP7*, and *IBSP* compared to the ST (+) group (Fig. 1c). On the other hand, the chondrocyte-related gene *COL2A1* was significantly upregulated in the ST (+) group, but not in the ST (−) group, compared to Day 0 and Day 5. A similar trend was observed in another hPSC line, Col2.3GFP-H9-hESCs [13,14] (Supplementary Fig. 1), indicating that the protocol works with no cell line-dependency. Collectively, these data suggest that the 14-day spheroid cultures of the hPSC-derived sclerotome generate skeletal progenitors with distinct characteristics; the ST (−) spheroid culture is likely suitable for the induction of an osteoprogenitor population, while the ST (+) culture predominantly induces osteo-chondroprogenitors and/or chondroprogenitors (Fig. 1d).

3.2. Characterization of the hPSC-derived skeletal progenitors in the spheroids

To further characterize the hiPSC-derived skeletal progenitors, we performed histological analyses of the spheroids. Hematoxylin and eosin (H-E) staining revealed that both ST (−) and ST (+) spheroids were predominantly composed of basophilic cells (Fig. 2a). In immunohistochemical analyses, RUNX2 and SP7, which are master regulators of osteogenesis, were expressed in both ST (−) and ST (+) spheroids (Fig. 2a). However, the expression of SOX9, a master regulator of chondrogenesis, was greater in the ST (+) spheroid (Fig. 2a). In addition, as we generated both ST (−) and ST (+) spheroids with sclerotome induced from WIZ04e-H9CAGmChry-hESCs [15], which express mCherry constitutively, we performed *in situ* hybridization in the hESC-derived spheroids; *COL1A1* expression was more dominant in the ST (−) spheroids, whereas *COL2A1* expression was observed only in the ST (+) spheroids (Fig. 2b). These data support the aforementioned notion that osteoprogenitors are dominant in the ST (−) spheroids, while the ST (+) spheroids contain osteo-chondroprogenitors and/or chondroprogenitors.

3.3. In vivo generation of bone tissues from the hPSC-derived skeletal progenitors

To test the *in vivo* ossification capacities of the hPSC-derived skeletal progenitors, we implanted the hiPSC-derived ST (−) or ST (+) spheroids beneath the renal capsule of immunodeficient mice (Fig. 3a). Gross appearance and 3D-μCT analyses indicated the presence of radiopaque bone-like structures on the surface of the kidney at 8 weeks after implantation in both of the ST (−) or ST (+) spheroid groups (Fig. 3b).

We attempted to identify the cellular characteristics of the bone-like structures by histological analyses at 8 weeks after implantation (Fig. 3b). H-E and Safranin-O (SO) staining showed that the ST (+) group generated cartilage tissues, whereas the ST (−) group did not (see H-E and SO in Fig. 3b); together with the 3D-μCT data, the H-E and SO staining results also suggested that the central part of the ST (−) group consisted of highly calcified tissues, which were surrounded by mesenchymal cells. Immunohistochemistry for human nuclei (HN) indicated that the structures were composed of human cells, i.e., hiPSC-derived cells, in both groups (see HN in Fig. 3b). In the ST (−) group, RUNX2-positive cells and SP7-positive ones were present at peripheral areas of the structures; the expression of SOX9 was weak or barely detectable (see RUNX2, SP7, and SOX9 of the left column in Fig. 3b). In the ST (+) group, the cartilage-like tissue, which appeared in red by SO staining, contained prehypertrophic and hypertrophic cells; those cells expressed RUNX2 and SP7 as well as SOX9 (see RUNX2, SP7, and SOX9 in the right column in Fig. 3b), as prehypertrophic and hypertrophic chondrocytes do in developing endochondral bones [31]. These data suggest that the ST (−) spheroids induced intramembranous ossification, while the ST (+) spheroids induced endochondral ossification.

Based on the above results, we next focused on the intramembranous ossification process induced by the ST (−) spheroids. At 12 weeks after the implantation, the bone-like structure appeared with blood vessels (Fig. 3c). It was composed of RUNX2- and SP7-positive cells (Fig. 3c). In contrast, SOX9 was barely detectable, just as it was in the 8-week sample (Fig. 3c). *In situ* hybridization further revealed that the osteocyte marker *SOST* was expressed in cells embedded in the bone-like structure (Fig. 3d), suggesting the presence of mature osteoblasts and osteocytes.

So far, the data collected on our present model suggest that we have successfully recapitulated intramembranous ossification in a 3D manner using osteoprogenitors induced from the hPSC-derived sclerotome, and that our spheroid culture will allow the hPSC-derived sclerotome to choose two distinct skeletal cell fates depending on the presence of the ST stimulus—i.e., osteoprogenitors and osteo-chondroprogenitors that can induce intramembranous and endochondral ossification *in vivo*, respectively.

3.4. Transcriptional profiling of the intramembranous bone-like tissues

Lastly, we performed bulk RNA-seq analysis to characterize the ST (−) spheroid-derived intramembranous bone-like tissues in terms of transcriptional profiles. We analyzed Day 0 (pluripotent state) and Day 5 (sclerotome population) samples in the culture as well as the intramembranous bone-like tissues collected at 8 weeks after implantation (called 8-wk tissues hereafter). Principal component analysis (PCA) indicated that the transcriptional profiles were distinct between groups and similar between replicates in each group (Fig. 4a). k-means clustering analysis revealed key

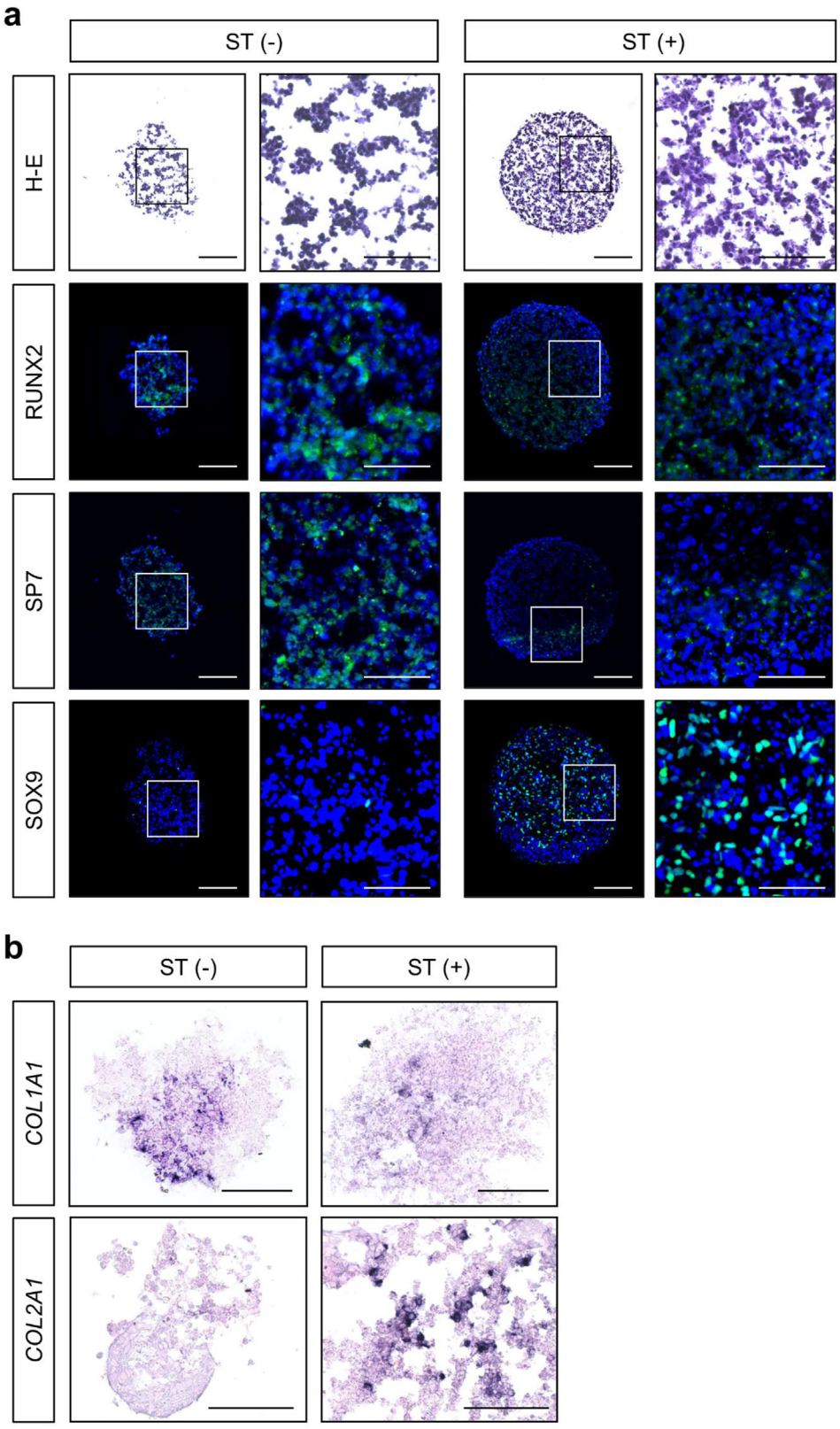

Fig. 2. Characterization of skeletal progenitors generated by the spheroid culture of hPSC-derived sclerotome. (a) Hematoxylin and eosin (H–E) staining and immunofluorescence for skeletal mater regulators (SOX9, RUNX2, and SP7) of the spheroids at Day 19 of the culture. Magnified views of rectangular areas are shown in right. The protein expression is indicated by green fluorescence, and nuclei are stained with DAPI. Scale bars, 100 μm (left, low magnification) and 50 μm (right, high magnification). (b) *In situ* hybridization for *COL1A1* and *COL2A1* in the spheroids generated from the WIZ04e-H9CAGmChry-hESC-derived sclerotome. Scale bars, 100 μm.

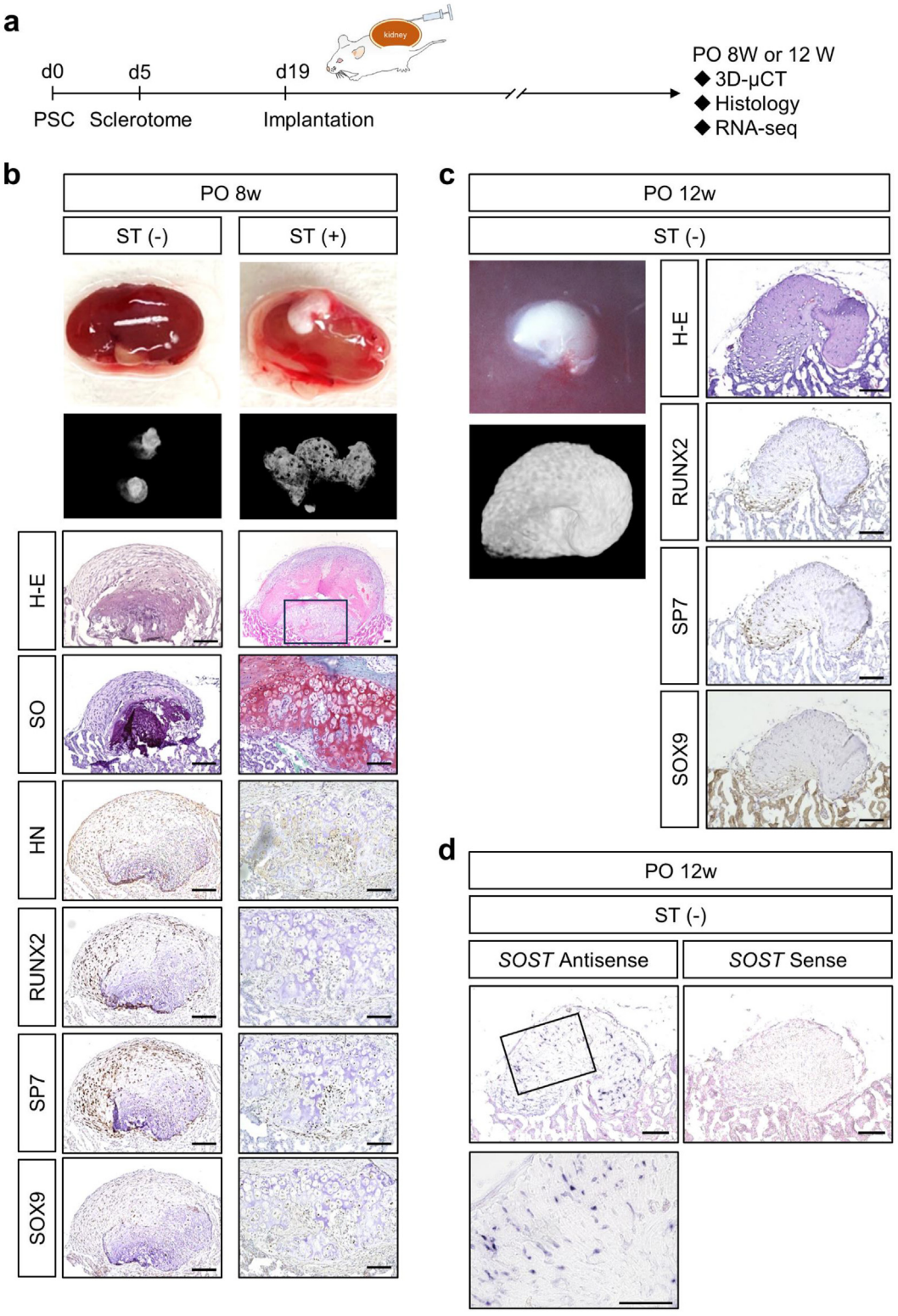

Fig. 3. Recapitulation of intramembranous and endochondral ossification by the hPSC-derived sclerotome. (a) A schematic showing the experimental procedure. After 19-day induction of skeletal progenitors, the hiPSC-derived spheroids were implanted beneath the renal capsule of immunodeficient mice. (b) Gross appearance, 3D-μCT images, and histological analyses of the induced tissues at 8 weeks after implantation. For histological analyses, H-E staining, safranin-O (SO) staining, and immunohistochemistry for human nuclei (HN) and skeletal master regulators (RUNX2, SP7, SOX9) were performed. Immunohistochemical signals are shown in brown. Scale bars, 100 μm. (c) Gross appearance, 3D-μCT images, and histological analyses of the tissues induced from an ST (−) spheroid at 12 weeks after implantation. Immunohistochemical signals are shown in brown. Scale bars, 100 μm. (d) *In situ* hybridization for *SOST* in the tissues induced from the ST (−) spheroid at 12 weeks after implantation. Hybridization signals are shown in blue. Scale bars, 100 μm. The magnified view of the region indicated by the rectangular box is also shown.

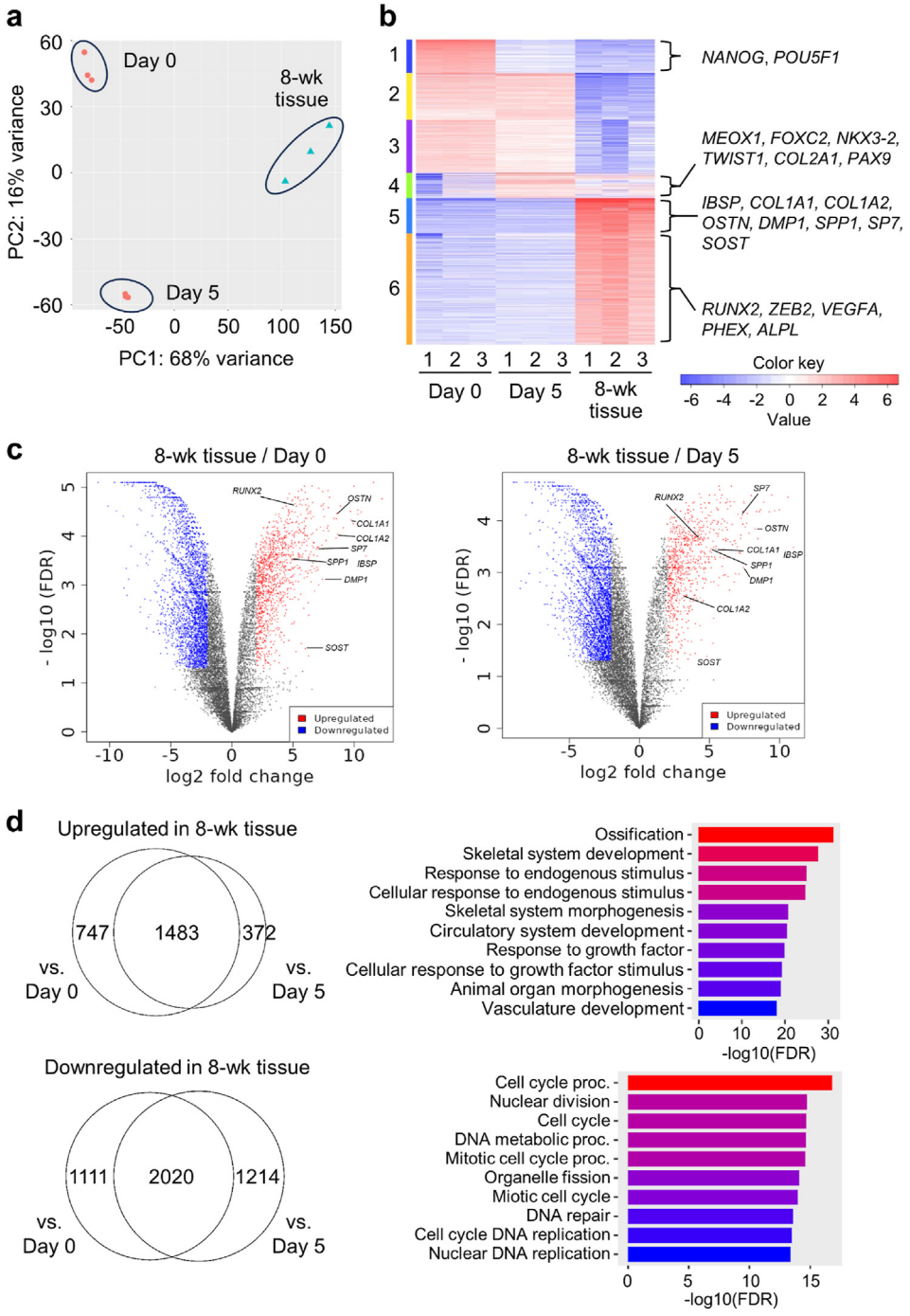

Fig. 4. Skeletal signatures identified by transcriptional profiling in the intramembranous bone-like tissues. (a) Principal component analysis (PCA) of the Day 0 (pluripotent state), Day 5 (sclerotome population), and 8-wk tissue (*in vivo* tissues induced at 8 weeks after implantation) data sets. (b) k-means clustering of the Day 0 (pluripotent state), Day 5 (sclerotome population), and 8-wk tissues (*in vivo* tissues induced at 8 weeks after implantation) data sets. (c) Volcano plot of differentially expressed genes (DEGs). Red and blue dots show genes upregulated and downregulated in 8-wk tissues, respectively. Key skeletal genes are marked. (d) Gene ontology (GO) analysis of upregulated and downregulated genes in 8-wk tissues compared to Day 0 and Day 5 samples. Genes that were commonly upregulated or downregulated in comparison with Day 0 and Day 5 samples were selected as DEGs and subjected to gene ontology analysis (GO biological process).

signatures in each of Day 0, Day 5, and 8-wk tissue samples (Fig. 4b and Supplementary Table 3). Cluster 1, which represents genes highly expressed at Day 0, contains pluripotency-related genes such as *NANOG* and *POU5F1* (also known as *OCT4*). Cluster 4, which represents genes highly expressed at Day 5, contains paraxial mesoderm-somite-sclerotome genes such as *MEOX1*, *FOXC2*, *NKX3-2*, *TWIST1*, *COL2A1*, and *PAX9*. Clusters 5 and 6, which represent genes highly expressed in the 8-wk tissues, are characterized by osteoblast and osteocyte-related genes such as *IBSP*, *COL1A1*, *COL1A2*, *OSTN*, *DMP1*, *SPP1*, *SP7*, *SOST*, *RUNX2*, *ZEB2*, *VEGFA*, *PHEX*, and *ALPL*. It is worth noting that *CTSK*, a marker of periosteal stem cells as well as osteoclasts [32], is found in Cluster 5, although the expression of other osteoclast-related genes, such as *TNFRSF11A* (also known as RANK), *ACP5* (also known as TRAP), *TNFSF11* (also

known as RANKL), and *TNFRSF11B* (also known as OPG), was barely or not at all detectable (Supplementary Table 4). Cluster 5 also contains periosteum- and fibroblast-related genes, such as *POSTN* (periostin), *DCN* (decorin), *ASPN* (asporin), and *COL3A1*.

We next identified differentially expressed genes (DEGs) in the 8-wk tissues compared to Day 0 or Day 5 samples. Osteoblast- and osteocyte-related genes were strongly upregulated in the 8-wk tissues (Fig. 4c and Supplementary Table 5). Among DEGs with FDR<0.05, genes with fold change>4 and those with fold change<0.25 in both the comparisons with Day 0 and those with Day 5 samples were selected as upregulated and downregulated gene sets, respectively (1483 and 2020 genes for the upregulated and downregulated genes, respectively) (Venn diagrams in Fig. 4d); we performed gene ontology analysis on both gene sets. Upregulated gene sets were highly enriched with genes related to bone-related terms: *Ossification*, *Skeletal system development*, and *Skeletal system morphogenesis* (upper right in Fig. 4d); in contrast, downregulated gene sets were enriched with genes related to mitosis-, cell cycle-, and DNA replication-related terms (lower right in Fig. 4d). This result suggests a cellular shift from mitotic progenitor states (Day 0 and Day 5) to differentiated mature states (8-wk tissues). Thus, the gene expression profiles support the idea that human bone tissues containing mature osteoblasts and osteocytes were generated, probably through the intramembranous ossification process.

4. Discussion

We have three major findings in this study. First, osteoprogenitor- and osteo-chondroprogenitor-like populations were selectively induced from the hPSC-derived sclerotome in our 3D culture; the former was predominantly induced in the absence of SAG and TH (ST (−)), whereas the latter was predominantly induced in the presence of the combination (ST (+)). Second, the induced cells formed bone-like structures with distinct modes of ossification *in vivo*; the ST (−) spheroids were likely to induce intramembranous ossification, while the ST (+) spheroids induced endochondral ossification. Third, bulk RNA-seq analysis supported the idea that osteoblasts and osteocytes were enriched in the ST (−) spheroid-derived bone-like structures. Thus, we have newly developed a system that recapitulates human intramembranous ossification *in vivo*. The data also suggest that our 3D culture permits the hPSC-derived sclerotome to choose two skeletal progenitor fates, which can direct distinct modes of ossification *in vivo*, depending on the presence of the ST stimulus.

We cultured the hPSC-derived sclerotome population under a defined 3D condition, aiming to mimic mesenchymal condensation processes and thereby augment the production of skeletal progenitors. The RT-qPCR results suggested that the 3D condition was suitable for the generation of skeletal progenitors from this population. In addition, the defined conditions are expected to enhance the reproducibility of our system without evoking the ethical issues that often arise in the study of human organogenesis. However, the biological mechanisms underlying the advantage of the 3D culture in skeletal cell differentiation remain to be investigated. One possible explanation is that the 3D culture reproduces a hypoxic condition similar to *in vivo* mesenchymal condensation [33], which may enhance differentiation into skeletal cells in the spheroids.

The ST treatment preferentially induced osteo-chondroprogenitors, which induced endochondral ossification *in vivo*. This result was not consistent with the initial hypothesis drawn from our previous findings [27–30], as mentioned in the Results section. Our hypothesis also relied on the notion that Indian hedgehog (Ihh) acts as a master regulator of osteoblast development [34,35]. In contrast, Sonic hedgehog (Shh), another Hh family member, has been shown to execute the chondrogenic program in somites [36,37]; in that model, Shh initiates a positive regulatory loop between Sox9 and Nkx3.2, which is maintained by BMP signaling. Given that SAG activates Hh signaling and TH has a BMP-dependent activity [38], it is possible that the ST treatment, in cooperation with endogenous BMPs, reproduces the initiation and maintenance of the regulatory loop and generates chondroprogenitors/osteo-chondroprogenitors from our hPSC-derived paraxial mesoderm derivatives. The biological mechanisms underlying osteoprogenitor induction in the ST (−) spheroids are still unclear, although components in the BIM medium may facilitate an osteoblast program in the absence of exogenous Hh inputs.

Histological analysis and RNA-seq analysis suggested that ST (−) spheroid-derived bone-like tissues are intramembranous bones containing mature osteoblasts and osteocytes. Osteocyte-related genes such as *SOST*, *OSTN*, *DMP1*, and *PHEX*, as well as osteoblast-related genes, were expressed at high levels in the tissue. Those genes represent important aspects of osteocyte biology, including bone metabolism (*SOST*) [39], dendrite formation (*OSTN*) [40], and phosphate metabolism (*DMP1* and *PHEX*). In contrast, *FGF23*, which is an osteocyte-releasing hormone regulating phosphate metabolism and a therapeutic target for vitamin D-resistant rickets/osteomalacia [41], was not detected in the tissue despite the substantial expression of the above osteocyte-related genes. These results suggest that the induced tissues reflect physiological osteocyte biology, given that the FGF23 expression level was considerably low in osteocytes in normal states [42].

CTSK, a marker for periosteal stem cells as well as osteoclasts [32], was highly expressed in the 8-wk tissues. Importantly, the expression of other osteoclast-related genes was low or barely detected, and periosteum/fibroblast-related genes were highly expressed. Thus, the *CTSK* expression may indicate the presence of periosteal stem cells in the tissues, although more precise characterization will be needed before drawing any definitive conclusions. The cells are thought to contribute to intramembranous ossification *in vivo* at a physiological state [32]; the presence of the population may partly account for the cellular mechanisms underlying our *in vivo* results. It is also worth noting that *ZEB2* was upregulated in the 8-wk tissues compared to the Day 5 sample. Heterozygous mutation or deletion of *ZEB2* causes Mowat-Wilson syndrome, whose clinical characteristics include craniofacial features [43]. We recently identified *ZEB2* as an osteogenic regulator through single-cell analysis on hPSC-derived bones [13]. Thus, upregulation of *ZEB2* may partly support the integrity of the induced tissues.

This study has two major limitations. First, our system may not completely recapitulate the physiological intramembranous ossification directed by paraxial mesoderm derivatives. The paraxial mesoderm-derived intramembranous bone (i.e., the parietal bone) is not formed by the somite−sclerotome [44]; unsegmented paraxial mesoderm is thought to contribute to head regions by moving dorsally around the brain, although several markers for somite are expressed in the head paraxial mesoderm-derived cells [44]. It is possible that our hPSC-derived population may, at least to some extent, contain the unsegmented paraxial mesoderm population and undergo the process of intramembranous ossification. Alternatively, our culture condition may force the hPSC-derived population to acquire another property to recapitulate the process. Second, several chondrocyte-related genes were upregulated in the 8-wk tissues compared to the Day 0 and Day 5 samples. These genes include *COL9A2*, *COL11A1*, *COL11A2*, and *ACAN*. In contrast, *SOX9* showed slight upregulation compared to Day 0 samples, but not Day 5 samples; its target *COL2A1* was upregulated compared to Day 0, but downregulated compared to Day 5. This result is, at least partly, consistent with our previous finding that osteoblasts express

chondrocyte-related genes at low levels [45]. Another possibility is that the tissues consist of heterogenous cell populations; some cells may partly execute the chondrocyte program. However, the osteoblast program is likely to be dominant in the tissue, leading to *in vivo* intramembranous ossification. We are planning to perform single-cell analysis on both spheroids and the induced tissues in the near future, which will provide clarification of these two issues.

5. Conclusions

We developed a hPSC-based system that recapitulates intramembranous ossification *in vivo*. The system also enables modeling of both intramembranous and endochondral ossification, depending on the spheroid culture conditions. Although several limitations need to be overcome, this work is an important first step to understand the human intramembranous ossification process. In addition, the system is expected to contribute to understanding of human osteocyte biology and osteocyte-related diseases, and thereby the development of novel therapeutics in skeletal fields.

Declaration of competing interest

The authors declare the following financial interests/personal relationships which may be considered as potential competing interests: Shinsuke Ohba reports financial support was provided by Japan Society for the Promotion of Science. Shinsuke Ohba reports financial support was provided by Uehara Memorial Foundation. Shinsuke Ohba reports financial support was provided by Koyanagi Foundation. Shinsuke Ohba reports financial support was provided by Takeda Science Foundation. Shinsuke Ohba reports financial support was provided by Naito Foundation. Hironori Hojo reports financial support was provided by Japan Society for the Promotion of Science. Hironori Hojo reports financial support was provided by Uehara Memorial Foundation. Ung-il Chung reports financial support was provided by Japan Society for the Promotion of Science.

Acknowledgements

We thank Drs. Hiroyuki Okada (The University of Tokyo) and Hirotaka Matsumoto (Nagasaki University) for support with the bioinformatic analysis, Dr. Tomohiro Konno (Tohoku University) for support with the preparation of MPC-coated plates, and Mariko Kasai for technical assistance. The super-computing system SHIROKANE was provided by the Human Genome Center at The University of Tokyo. This study was funded by Grants-in-Aid for Scientific Research from the Japan Society for the Promotion of Science (JSPS: 21H04952, 21H03142, 21K19611, 20H03885), a Uehara Memorial Foundation Research Grant (to S.O. and H.H.), a Koyanagi Foundation Research Grant (to S.O.), a Naito Foundation Research Grant (to S.O.), and a Takeda Science Foundation Research Grant (to S.O.).

Appendix A. Supplementary data

Supplementary data to this article can be found online at https://doi.org/10.1016/j.reth.2023.09.017.

References

[1] Galea GL, Zein MR, Allen S, Francis-West P. Making and shaping endochondral and intramembranous bones. Dev Dynam 2021;250:414–49.
[2] Ohba S. Genome-scale actions of master regulators directing skeletal development. Jpn Dent Sci Rev 2021;57:217–23.
[3] Tani S, Chung UI, Ohba S, Hojo H. Understanding paraxial mesoderm development and sclerotome specification for skeletal repair. Exp Mol Med 2020;52:1166–77.
[4] De Kinderen P, Meester J, Loeys B, Peeters S, Gouze E, Woods S, et al. Differentiation of induced pluripotent stem cells into chondrocytes: methods and applications for disease modeling and drug discovery. J Bone Miner Res 2022;37:397–410.
[5] Humphreys PA, Mancini FE, Ferreira MJS, Woods S, Ogene L, Kimber SJ. Developmental principles informing human pluripotent stem cell differentiation to cartilage and bone. Semin Cell Dev Biol 2022;127:17–36.
[6] Loh KM, Chen A, Koh PW, Deng TZ, Sinha R, Tsai JM, et al. Mapping the pairwise choices leading from pluripotency to human bone, heart, and other mesoderm cell types. Cell 2016;166:451–67.
[7] Wu CL, Dicks A, Steward N, Tang R, Katz DB, Choi YR, et al. Single cell transcriptomic analysis of human pluripotent stem cell chondrogenesis. Nat Commun 2021;12:362.
[8] Umeda K, Zhao J, Simmons P, Stanley E, Elefanty A, Nakayama N. Human chondrogenic paraxial mesoderm, directed specification and prospective isolation from pluripotent stem cells. Sci Rep 2012;2:455.
[9] Dicks A, Wu CL, Steward N, Adkar SS, Gersbach CA, Guilak F. Prospective isolation of chondroprogenitors from human iPSCs based on cell surface markers identified using a CRISPR-Cas9-generated reporter. Stem Cell Res Ther 2020;11:66.
[10] Craft AM, Rockel JS, Nartiss Y, Kandel RA, Alman BA, Keller GM. Generation of articular chondrocytes from human pluripotent stem cells. Nat Biotechnol 2015;33:638–45.
[11] Xi H, Fujiwara W, Gonzalez K, Jan M, Liebscher S, Van Handel B, et al. In vivo human somitogenesis guides somite development from hPSCs. Cell Rep 2017;18:1573–85.
[12] Kidwai F, Mui BWH, Arora D, Iqbal K, Hockaday M, de Castro Diaz LF, et al. Lineage-specific differentiation of osteogenic progenitors from pluripotent stem cells reveals the FGF1-RUNX2 association in neural crest-derived osteoprogenitors. Stem Cell 2020;38:1107–23.
[13] Tani S, Okada H, Onodera S, Chijimatsu R, Seki M, Suzuki Y, et al. Stem cell-based modeling and single-cell multiomics reveal gene-regulatory mechanisms underlying human skeletal development. Cell Rep 2023;42:112276.
[14] Xin X, Jiang X, Wang L, Stover ML, Zhan S, Huang J, et al. A site-specific integrated Col2.3GFP reporter identifies osteoblasts within mineralized tissue formed in vivo by human embryonic stem cells. Stem Cells Transl Med 2014;3:1125–37.
[15] Chen Y, Xiong M, Dong Y, Haberman A, Cao J, Liu H, et al. Chemical control of grafted human PSC-derived neurons in a mouse model of Parkinson's disease. Cell Stem Cell 2016;18:817–26.
[16] Livak KJ, Schmittgen TD. Analysis of relative gene expression data using real-time quantitative PCR and the 2(-Delta Delta C(T)) Method. Methods 2001;25:402–8.
[17] Kawai S, Takagi Y, Kaneko S, Kurosawa T. Effect of three types of mixed anesthetic agents alternate to ketamine in mice. Exp Anim 2011;60:481–7.
[18] Abe M, Michikami I, Fukushi T, Abe A, Maeda Y, Ooshima T, et al. Hand2 regulates chondrogenesis in vitro and in vivo. Bone 2010;46:1359–68.
[19] Wu X, Howard MJ. Transcripts encoding HAND genes are differentially expressed and regulated by BMP4 and GDNF in developing avian gut. Gene Expr 2002;10:279–93.
[20] Fujikawa J, Tanaka M, Itoh S, Fukushi T, Kurisu K, Takeuchi Y, et al. Kruppel-like factor 4 expression in osteoblasts represses osteoblast-dependent osteoclast maturation. Cell Tissue Res 2014;358:177–87.
[21] Bolger AM, Lohse M, Usadel B. Trimmomatic: a flexible trimmer for Illumina sequence data. Bioinformatics 2014;30:2114–20.
[22] Dobin A, Davis CA, Schlesinger F, Drenkow J, Zaleski C, Jha S, et al. STAR: ultrafast universal RNA-seq aligner. Bioinformatics 2013;29:15–21.
[23] Liao Y, Smyth GK, Shi W. featureCounts: an efficient general purpose program for assigning sequence reads to genomic features. Bioinformatics 2014;30:923–30.
[24] Love MI, Huber W, Anders S. Moderated estimation of fold change and dispersion for RNA-seq data with DESeq2. Genome Biol 2014;15:550.
[25] Ge SX, Son EW, Yao R. iDEP: an integrated web application for differential expression and pathway analysis of RNA-Seq data. BMC Bioinf 2018;19:534.
[26] Ge SX, Jung D, Yao R. ShinyGO: a graphical gene-set enrichment tool for animals and plants. Bioinformatics 2020;36:2628–9.
[27] Maeda Y, Hojo H, Shimohata N, Choi S, Yamamoto K, Takato T, et al. Bone healing by sterilizable calcium phosphate tetrapods eluting osteogenic molecules. Biomaterials 2013;34:5530–7.
[28] Kanke K, Masaki H, Saito T, Komiyama Y, Hojo H, Nakauchi H, et al. Stepwise differentiation of pluripotent stem cells into osteoblasts using four small molecules under serum-free and feeder-free conditions. Stem Cell Rep 2014;2:751–60.
[29] Zujur D, Kanke K, Lichtler AC, Hojo H, Chung UI, Ohba S. Three-dimensional system enabling the maintenance and directed differentiation of pluripotent stem cells under defined conditions. Sci Adv 2017;3:e1602875.
[30] Zujur D, Kanke K, Onodera S, Tani S, Lai J, Azuma T, et al. Stepwise strategy for generating osteoblasts from human pluripotent stem cells under fully defined

xeno-free conditions with small-molecule inducers. Regen Ther 2020;14:19–31.
[31] Ohba S, He X, Hojo H, McMahon AP. Distinct transcriptional programs underlie Sox9 regulation of the mammalian chondrocyte. Cell Rep 2015;12:229–43.
[32] Debnath S, Yallowitz AR, McCormick J, Lalani S, Zhang T, Xu R, et al. Discovery of a periosteal stem cell mediating intramembranous bone formation. Nature 2018;562:133–9.
[33] Percival CJ, Richtsmeier JT. Angiogenesis and intramembranous osteogenesis. Dev Dynam 2013;242:909–22.
[34] Ohba S. Hedgehog signaling in skeletal development: roles of Indian hedgehog and the mode of its action. Int J Mol Sci 2020;21.
[35] St-Jacques B, Hammerschmidt M, McMahon AP. Indian hedgehog signaling regulates proliferation and differentiation of chondrocytes and is essential for bone formation. Genes Dev 1999;13:2072–86.
[36] Murtaugh LC, Chyung JH, Lassar AB. Sonic hedgehog promotes somitic chondrogenesis by altering the cellular response to BMP signaling. Genes Dev 1999;13:225–37.
[37] Zeng L, Kempf H, Murtaugh LC, Sato ME, Lassar AB. Shh establishes an Nkx3.2/Sox9 autoregulatory loop that is maintained by BMP signals to induce somitic chondrogenesis. Genes Dev 2002;16:1990–2005.
[38] Ohba S, Nakajima K, Komiyama Y, Kugimiya F, Igawa K, Itaka K, et al. A novel osteogenic helioxanthin-derivative acts in a BMP-dependent manner. Biochem Biophys Res Commun 2007;357:854–60.
[39] Tanaka S, Matsumoto T. Sclerostin: from bench to bedside. J Bone Miner Metabol 2021;39:332–40.
[40] Wang JS, Kamath T, Mazur CM, Mirzamohammadi F, Rotter D, Hojo H, et al. Control of osteocyte dendrite formation by Sp7 and its target gene osteocrin. Nat Commun 2021;12:6271.
[41] Kinoshita Y, Fukumoto S. X-linked hypophosphatemia and FGF23-related hypophosphatemic diseases: prospect for new treatment. Endocr Rev 2018;39:274–91.
[42] Liu S, Zhou J, Tang W, Jiang X, Rowe DW, Quarles LD. Pathogenic role of Fgf23 in hyp mice. Am J Physiol Endocrinol Metab 2006;291:E38–49.
[43] Garavelli L, Mainardi PC. Mowat-Wilson syndrome. Orphanet J Rare Dis 2007;2:42.
[44] Noden DM, Trainor PA. Relations and interactions between cranial mesoderm and neural crest populations. J Anat 2005;207:575–601.
[45] Hojo H, Ohba S, He X, Lai LP, McMahon AP. Sp7/Osterix is restricted to bone-forming vertebrates where it acts as a dlx Co-factor in osteoblast specification. Dev Cell 2016;37:238–53.